Appendix to "The evolution of strained turbulent plane wakes"

By M. M. Rogers

Journal of Fluid Mechanics, vol. 463 (2002), pp. 53–120.

Appendix B. Details of the numerical method

Following Rogallo (1977, 1981), consider a spatially linear mean flow component

$$\overline{U_i} = \overline{U_{i,j}} x_j = a_{ij} x_j \ , \tag{B 1}$$

where $a_{ij} = \overline{U_{i,j}}$ depends only on the time t. Decomposing into this mean field and a "fluctuating" field (which may have a mean component, such as the wake mean shear in the cases considered in this paper) one has

$$u_i(\vec{x}) = a_{ij} x_j + \tilde{u}_i(\vec{\tilde{x}}) \tag{B 2a}$$

$$p(\vec{x}) = \overline{P}(\vec{x}) + \tilde{p}(\vec{\tilde{x}}) \ , \tag{B 2b}$$

where the tilde coordinate system follows the linear mean flow (strain) according to

$$\tilde{x}_i = B_{ij}(t) x_j \tag{B 3a}$$

$$\dot{B}_{ij} + B_{ik} a_{kj} = 0 \ , \tag{B 3b}$$

and the overdot indicates differentiation with respect to time. For the case of a uniform irrotational strain, equation (B 3b) leads to

$$B_{11}(t) = B_{11}^0 \exp\left(- \int_0^t a_{11}(t') dt' \right) \ , \tag{B 4}$$

where $B_{11}^0 = B_{11}(t=0)$ and similar expressions hold for B_{22} and B_{33} (with a_{22} and a_{33} replacing a_{11}, respectively). After some manipulation, the continuity equation (2.1) and momentum equation (2.2) become

$$\tilde{u}_{i,\bar{j}} B_{ji} = 0 \tag{B 5}$$

$$\frac{\partial \tilde{u}_i}{\partial t} + a_{ij}\tilde{u}_j + B_{kj}(\tilde{u}_i \tilde{u}_j)_{,\bar{k}} + \frac{1}{\rho} B_{ji} \tilde{p}_{,\bar{j}} = \nu B_{kj} B_{lj} \tilde{u}_{i,\bar{k}\bar{l}} \ , \tag{B 6}$$

with the evolution of the explicit mean field being given by

$$[\dot{a}_{ik} + a_{ij} a_{jk}] x_k + \frac{1}{\rho} \overline{P}_{,i} = 0 \ , \tag{B 7}$$

the solution of which, for the case of irrotational strain, is given by equation (2.8). Equation (2.15) governing the Reynolds stress evolution transforms to

$$\begin{aligned} \frac{\partial \overline{u_i' u_j'}}{\partial t} = & - a_{ik} \overline{u_j' u_k'} - a_{jk} \overline{u_i' u_k'} - \left(\overline{u_i' u_l'} B_{kl} \frac{\partial \overline{U_j}}{\partial x_k} + \overline{u_j' u_l'} B_{kl} \frac{\partial \overline{U_i}}{\partial x_k} \right) - B_{kl} \frac{\partial \overline{u_i' u_j' u_l'}}{\partial x_k} \\ & + \overline{\frac{p'}{\rho} \left(B_{kj} \frac{\partial u_i'}{\partial x_k} + B_{ki} \frac{\partial u_j'}{\partial x_k} \right)} - \frac{1}{\rho} \left(B_{kj} \frac{\partial \overline{p' u_i'}}{\partial x_k} + B_{ki} \frac{\partial \overline{p' u_j'}}{\partial x_k} \right) \end{aligned}$$

$$+ \nu B_{lm} B_{km} \frac{\partial^2 \overline{u_i' u_j'}}{\partial x_k \partial x_l} - \nu B_{lm} B_{km} \left(\overline{\frac{\partial u_i'}{\partial x_k} \frac{\partial u_j'}{\partial x_l}} + \overline{\frac{\partial u_i'}{\partial x_l} \frac{\partial u_j'}{\partial x_k}} \right) , \tag{B 8}$$

where the tildes have been omitted for simplicity and $\overline{U_i}$ no longer includes the mean flow associated with the transformation (just the wake shear for the case considered here). Note that the strain production of turbulence now appears explicitly in the equation and that the convective part of the substantial derivative is zero in this coordinate system "moving" with the mean flow. A similar analysis of the rotational form of the Navier–Stokes equations yields

$$\frac{\partial \tilde{u}_i}{\partial t} + a_{ji} \tilde{u}_j - (\vec{\tilde{u}} \times \vec{\tilde{\omega}})_i + B_{ji} (\frac{1}{\rho} \tilde{p} + \frac{\tilde{u}_k \tilde{u}_k}{2})_{,\bar{j}} = \nu B_{kj} B_{lj} \tilde{u}_{i,\bar{k}\bar{l}} , \tag{B 9}$$

where, for the case of irrotational strain, the same mean equation (B 7) applies. Note that for irrotational strain $a_{ij} = a_{ji}$ and the linear terms of equations (B 6) and (B 9) are the same. The Reynolds stress evolution equation associated with this form of the Navier–Stokes equations is

$$\begin{aligned} \frac{\partial \overline{u_i' u_j'}}{\partial t} = & - a_{ki} \overline{u_j' u_k'} - a_{kj} \overline{u_i' u_k'} + \overline{u_i' (\vec{u} \times \vec{\omega})_j'} + \overline{u_j' (\vec{u} \times \vec{\omega})_i'} \\ & - \overline{u_i' B_{kj} \frac{\partial (p'/\rho + q^2/2)}{\partial x_k}} - \overline{u_j' B_{ki} \frac{\partial (p'/\rho + q^2/2)}{\partial x_k}} \\ & + \nu B_{lm} B_{km} \frac{\partial^2 \overline{u_i' u_j'}}{\partial x_k \partial x_l} - \nu B_{lm} B_{km} \left(\overline{\frac{\partial u_i'}{\partial x_k} \frac{\partial u_j'}{\partial x_l}} + \overline{\frac{\partial u_i'}{\partial x_l} \frac{\partial u_j'}{\partial x_k}} \right) , \end{aligned} \tag{B 10}$$

where again the tildes have been omitted for simplicity.

Similarly, the evolution equation for the vorticity ($\tilde{\omega}_i = \epsilon_{ijk} B_{lj} \tilde{u}_{k,\bar{l}}$) in "rotational" form transforms to

$$\frac{\partial \tilde{\omega}_i}{\partial t} = a_{ij} \tilde{\omega}_j + \epsilon_{ijk} B_{lj} (\vec{\tilde{u}} \times \vec{\tilde{\omega}})_{k,\bar{l}} + \nu B_{kj} B_{lj} \tilde{\omega}_{i,\bar{k}\bar{l}} , \tag{B 11}$$

where ϵ_{ijk} is the alternating symbol defined to be one if the subscripts i, j, k are in cyclic order, -1 if they are in anti-cyclic order, and 0 otherwise (if two or more suffixes are the same). No equation governing the mean vorticity associated with the transformation is required because it is zero for the irrotational strains considered here.

Decomposing the passive scalar quantity into a uniform (but time-evolving) mean scalar gradient and "fluctuations" in the moving coordinate system we have

$$T(\vec{x}) = \overline{T}_{,j}(t) x_j + \tilde{\theta}(\vec{\tilde{x}}) . \tag{B 12}$$

The equation governing the scalar fluctuations is then given by

$$\frac{\partial \tilde{\theta}}{\partial t} + \overline{T}_{,j} \tilde{u}_j + B_{ji} \tilde{u}_i \tilde{\theta}_{,\bar{j}} = \gamma B_{kj} B_{lj} \tilde{\theta}_{,\bar{k}\bar{l}} , \tag{B 13}$$

where $\overline{T}$ here includes only that portion of the mean scalar associated with the transformation and is governed by the constraint

$$\dot{\overline{T}}_{,j} + a_{ij} \overline{T}_{,i} = 0 , \tag{B 14}$$

which has as its solution for the case of irrotational mean strain

$$\overline{T}_{,1} = \overline{T}_{,1}(t=0) e^{-a_{11} t} , \tag{B 15}$$

where similar equations apply for $\overline{T}_{,2}$ and $\overline{T}_{,3}$ with a_{22} and a_{33} replacing a_{11}, respectively.

It should be noted that if there is a non-periodic component to the mean velocity in the strained coordinate system, then an equation similar to equation (B 15) applies to the explicitly carried non-periodic portion of this mean. For example, consider a strained mixing layer, which has a mean velocity difference across the layer in addition to the mean flow associated with the global strain. In this case the non-periodic function $U_e(y,t)$ explicitly carried to account for the non-periodic boundary conditions evolves according to

$$U_e(y,t) = U_e(y,t=0)e^{-a_{11}t} \; . \tag{B 16}$$

If $a_{11} = 0$ the explicitly carried function is constant as in the unstrained cases. Otherwise, the explicitly carried velocity difference must change in time as given by equation (B 16). The analytical solutions for laminar strained free shear layers given in Appendix C are useful for understanding this and for testing codes developed to simulate these flows.

As done in Spalart *et al.* (1991), after Fourier transforming in x and z (yielding $\widehat{\omega}_i$), the vorticity is projected into a coordinate system parallel and perpendicular to the (k_x,k_z) wavevector. However, this projection now includes the effect of the B_{ij}'s associated with the strain:

$$\widehat{\omega}^{\parallel} \equiv \frac{B_{11}k_x\widehat{\omega}_x + B_{33}k_z\widehat{\omega}_z}{k} \tag{B 17a}$$

$$\widehat{\omega}^{\perp} \equiv \frac{-B_{33}k_z\widehat{\omega}_x + B_{11}k_x\widehat{\omega}_z}{k} \; , \tag{B 17b}$$

where $k = \sqrt{B_{11}^2k_x^2 + B_{33}^2k_z^2}$ and both the tildes indicating the moving coordinate system and the primes indicating turbulence fluctuations have been dropped (all equations given below are in this moving frame and deal with fluctuating quantities). The solenoidal character of the vorticity is expressed as

$$ik\widehat{\omega}^{\parallel} + B_{22}\frac{\partial\widehat{\omega}_y}{\partial y} = 0 \; , \tag{B 18}$$

the kinematic relationship between the vorticity and the velocity is given by

$$-ik\widehat{u}^{\perp} = \widehat{\omega}_y \tag{B 19a}$$

$$\nabla^2\widehat{v} = B_{22}^2\frac{\partial^2\widehat{v}}{\partial y^2} - k^2\widehat{v} = ik\widehat{\omega}^{\perp} \; , \tag{B 19b}$$

and continuity requires that

$$ik\widehat{u}^{\parallel} + B_{22}\frac{\partial\widehat{v}}{\partial y} = 0 \; , \tag{B 20}$$

where again k is modified as above to include the B_{ij}'s. Note that for the mean flow ($k_x = 0$, $k_z = 0$) the projection (B 17) is undefined. For this mode the equation (B 9) is used to advance the $\overline{U}$ and $\overline{W}$ velocities as in Spalart *et al.* (1991).

The governing equations for $\widehat{\omega}^{\parallel}$ and $\widehat{\omega}^{\perp}$ can be obtained from those for $\widehat{\omega}_x$ and $\widehat{\omega}_z$ (equation (B 11), keeping in mind that k and B_{ij} are functions of time. This results in the set of equations

$$\begin{aligned}\frac{\partial\widehat{\omega}^{\parallel}}{\partial t} &= B_{22}\frac{\partial}{\partial y}(\overrightarrow{u}\times\overrightarrow{\omega})^{\perp} + \nu\left(B_{22}^2\frac{\partial^2\widehat{\omega}^{\parallel}}{\partial y^2} - k^2\widehat{\omega}^{\parallel}\right) \\ &\quad + \frac{B_{11}^2k_x^2a_{11} + B_{33}^2k_z^2a_{33}}{k^2}\widehat{\omega}^{\parallel}\end{aligned} \tag{B 21}$$

$$\frac{\partial\widehat{\omega}_y}{\partial t} = a_{22}\widehat{\omega}_y - ik(\overrightarrow{u}\times\overrightarrow{\omega})^{\perp} + \nu\left(B_{22}^2\frac{\partial^2\widehat{\omega}_y}{\partial y^2} - k^2\widehat{\omega}_y\right) \tag{B 22}$$

$$\frac{\partial \widehat{\omega}^{\perp}}{\partial t} = -B_{22}\frac{\partial}{\partial y}(\overrightarrow{u}\times\overrightarrow{\omega})^{\parallel} + ik(\overrightarrow{u}\times\overrightarrow{\omega})_2 + \nu\left(B_{22}^2\frac{\partial^2\widehat{\omega}^{\perp}}{\partial y^2} - k^2\widehat{\omega}^{\perp}\right) + \frac{B_{11}^2k_x^2a_{33} + B_{33}^2k_z^2a_{11}}{k^2}\widehat{\omega}^{\perp} + \frac{2B_{11}B_{33}k_xk_z(a_{33}-a_{11})}{k^2}\widehat{\omega}^{\parallel}\,, \tag{B 23}$$

where only the $\widehat{\omega}_y$ and $\widehat{\omega}^{\perp}$ equations are advanced computationally ($\widehat{\omega}^{\parallel}$ being determined from the solenoidal character of the vorticity field, equation (B 18). In the above equations and below the quantity $(\overrightarrow{u}\times\overrightarrow{\omega})_i$ is the (k_x,k_z) Fourier transform of the i^{th} component of the fluctuating (turbulent) part of the cross product of u and ω, where in this instance u and ω include any mean component not explicitly accounted for by the transformation. This term can be written as

$$(\overrightarrow{u}\times\overrightarrow{\omega})_i = B_{ji}(u_ku_k/2)_{,j} - B_{jk}(u_iu_k)_{,j}\,, \tag{B 24}$$

where the projection in equation (B 17) can be used to obtain $(\overrightarrow{u}\times\overrightarrow{\omega})^{\parallel}$ and $(\overrightarrow{u}\times\overrightarrow{\omega})^{\perp}$. Note that from all these equations the unstrained wake equations used to generate the simulations in Moser *et al.* (1998) can be recovered by taking $B_{ij}=\delta_{ij}$ and setting $a_{ij}=0$.

Besides the Poisson equation given in equation (B 19b), the following Poisson equations are useful for consistently computing various statistics in the Reynolds stress balance:

$$\nabla^2\widehat{u}^{\parallel} = -B_{22}\frac{\partial\widehat{\omega}^{\perp}}{\partial y} \tag{B 25}$$

$$\nabla^2\frac{\partial\widehat{v}}{\partial t} = ik\frac{\partial\widehat{\omega}^{\perp}}{\partial t} + 2\widehat{v}(B_{11}^2k_x^2(a_{22}-a_{11}) + B_{33}^2k_z^2(a_{22}-a_{33})) + \frac{i\widehat{\omega}^{\perp}}{k}(B_{11}^2k_x^2(2a_{22}-a_{11}) + B_{33}^2k_z^2(2a_{22}-a_{33})) \tag{B 26}$$

$$\nabla^2\frac{\partial\widehat{u}^{\parallel}}{\partial t} = -B_{22}\frac{\partial}{\partial y}\frac{\partial\widehat{\omega}^{\perp}}{\partial t} - B_{22}a_{22}\frac{\partial\widehat{\omega}^{\perp}}{\partial y} + 2\widehat{u}^{\parallel}(B_{11}^2k_x^2(a_{22}-a_{11}) + B_{33}^2k_z^2(a_{22}-a_{33})) \tag{B 27}$$

$$\nabla^2(p/\rho) = -B_{ji}B_{kl}\frac{\partial\widehat{u}_i}{\partial x_k}\frac{\partial\widehat{u}_l}{\partial x_j} - 2B_{ji}a_{ik}\frac{\partial\widehat{u}_k}{\partial x_j} \tag{B 28}$$

$$\nabla^2(p/\rho+\widehat{u}_k\widehat{u}_k/2) = B_{ji}\frac{\partial}{\partial x_j}(\overrightarrow{u}\times\overrightarrow{\omega})_i - 2B_{ji}a_{ki}\frac{\partial\widehat{u}_k}{\partial x_j} \tag{B 29}$$

$$\nabla^2B_{22}\frac{\partial}{\partial y}(p/\rho+\widehat{u}_k\widehat{u}_k/2) = B_{22}\frac{\partial}{\partial y}B_{ji}\frac{\partial}{\partial x_j}(\overrightarrow{u}\times\overrightarrow{\omega})_i - 2B_{22}\frac{\partial\widehat{\omega}_y}{\partial y}\frac{B_{11}B_{33}k_xk_z(a_{11}-a_{33})}{k^2} + 2B_{22}^2\frac{\partial^2\widehat{v}}{\partial y^2}\frac{B_{11}^2k_x^2(a_{11}-a_{22}) + B_{33}^2k_z^2(a_{33}-a_{22})}{k^2}\,. \tag{B 30}$$

Note that in all these cases ∇^2 includes the B_{ij}'s as defined in equation (B 19b). To recover the time derivatives of the velocity components u and w, the projection expressions

$$\widehat{u} = \frac{B_{11}k_x\widehat{u}^{\parallel} - B_{33}k_z\widehat{u}^{\perp}}{k} \tag{B 31a}$$

$$\widehat{w} = \frac{B_{33}k_z\widehat{u}^{\parallel} + B_{11}k_x\widehat{u}^{\perp}}{k} \tag{B 31b}$$

can be used to find that

$$\frac{\partial\widehat{u}}{\partial t} = \frac{B_{11}k_x}{k}\frac{\partial\widehat{u}^{\parallel}}{\partial t} - \frac{iB_{33}k_z}{k^2}\frac{\partial\widehat{\omega}_y}{\partial t} + \frac{B_{11}B_{33}^2k_xk_z^2(a_{33}-a_{11})}{k^3}\widehat{u}^{\parallel}$$

$$+\frac{iB_{33}k_z}{k^2}\frac{B_{11}^2k_x^2(a_{33}-2a_{11})-B_{33}^2k_z^2a_{33}}{k^2}\widehat{\omega}_y \tag{B 32}$$

$$\frac{\partial\widehat{w}}{\partial t}=\frac{B_{33}k_z}{k}\frac{\partial\widehat{u}^{\parallel}}{\partial t}+\frac{iB_{11}k_x}{k^2}\frac{\partial\widehat{\omega}_y}{\partial t}+\frac{B_{11}^2B_{33}k_x^2k_z(a_{11}-a_{33})}{k^3}\widehat{u}^{\parallel}$$
$$+\frac{iB_{11}k_x}{k^2}\frac{B_{11}^2k_x^2a_{11}-B_{33}^2k_z^2(2a_{33}-a_{11})}{k^2}\widehat{\omega}_y\ . \tag{B 33}$$

As always, the unstrained expressions can be recovered by setting $B_{ij}=\delta_{ij}$ and $a_{ij}=0$.

The method of Corral & Jimenez (1995) can be extended to the moving coordinate system by "matching" at a cross-stream domain boundary that is fixed (at $\pm\pi$) in the "moving" cross-stream coordinate. As noted above, Fourier modes are used to represent the vorticity in this transformed direction; thus equation (B 19b) can be written as

$$\widehat{v}_{per}=-\frac{ik}{K^2}\widehat{\omega}^{\perp}\ , \tag{B 34}$$

where $K=\sqrt{B_{11}^2k_x^2+B_{22}^2k_y^2+B_{33}^2k_z^2}$ and v_{per} is the cross-stream velocity associated with the periodic array of vorticity fields. The actual cross-stream velocity must be determined by adding the appropriate amount of a potential solution v_{pot} (where $-K^2\widehat{v}_{pot}=0$) to obtain the correct non-periodic boundary conditions. The solution is given by

$$\widehat{v}=\widehat{v}_{per}+\widehat{v}_{pot} \tag{B 35a}$$
$$=\widehat{v}_{per}+A_2e^{-ky/B_{22}}+A_3e^{ky/B_{22}}\ , \tag{B 35b}$$

where A_2 and A_3 are determined by ensuring that the boundary values of the above solution and its gradient are the same as those given by the far-field potential solutions

$$\widehat{v}=A_1e^{-ky/B_{22}}\qquad y>\pi \tag{B 36a}$$
$$\widehat{v}=A_4e^{ky/B_{22}}\qquad y<-\pi\ . \tag{B 36b}$$

Higher-order derivatives will also be continuous because the vorticity and its derivatives are zero at the boundary. Defining

$$v_p=\widehat{v}_{per}(y=\pi)=\widehat{v}_{per}(y=-\pi) \tag{B 37a}$$
$$v_p'=\frac{\partial\widehat{v}_{per}}{\partial y}(y=\pi)=\frac{\partial\widehat{v}_{per}}{\partial y}(y=-\pi)\ , \tag{B 37b}$$

yields

$$A_1=\sinh(k\pi/B_{22})\left(v_p-\frac{B_{22}}{k}v_p'\right) \tag{B 38a}$$
$$A_2=\frac{e^{-k\pi/B_{22}}}{2}\left(-v_p+\frac{B_{22}}{k}v_p'\right) \tag{B 38b}$$
$$A_3=\frac{e^{-k\pi/B_{22}}}{2}\left(-v_p-\frac{B_{22}}{k}v_p'\right) \tag{B 38c}$$
$$A_4=\sinh(k\pi/B_{22})\left(v_p+\frac{B_{22}}{k}v_p'\right) \tag{B 38d}$$

Thus the potential correction to the periodic velocity component inside the computational domain is given by

$$\widehat{v}_{pot}=\frac{e^{-k(y+\pi)/B_{22}}}{2}\left(-v_p+\frac{B_{22}}{k}v_p'\right)+\frac{e^{k(y-\pi)/B_{22}}}{2}\left(-v_p-\frac{B_{22}}{k}v_p'\right)\ . \tag{B 39}$$

Appendix C. Analytical solutions

The solution given by Kambe & Minota (1983) for viscous two-dimensional flow in free space can be used to obtain solutions to the Navier–Stokes equations for viscous laminar free shear layers subjected to a strain given by $a_{11} = a$, $a_{22} = -a$, and $a_{33} = 0$ (the strain geometry used for cases C and D of the computations). Applying such a strain at time $t = 0$ to a laminar time-developing mixing layer with initial profile $\overline{U_1} = U_0 \mathrm{erf}(\sqrt{\pi} y/\delta_\omega^0)$, δ_ω^0 being the initial vorticity thickness and U_0 being half the initial velocity difference across the mixing layer, results in

$$\overline{U_1} = ax + U_m \mathrm{erf}\left(\frac{\sqrt{\pi} e^{at}}{\sqrt{1 + \frac{1}{Re}\left(e^{2at} - 1\right)}} \frac{y}{\delta_\omega^0} \right) \tag{C 1a}$$

$$\overline{U_2} = -ay \ , \tag{C 1b}$$

where the half-velocity difference U_m is given by

$$U_m = U_0 e^{-at} \tag{C 2}$$

and $Re = a(\delta_\omega^0)^2/(2\pi\nu)$ is a Reynolds number. From this solution the time-evolving vorticity thickness of the mixing layer component of the flow is determined to be

$$\delta_\omega = \delta_\omega^0 \frac{\sqrt{1 + \frac{1}{Re}\left(e^{2at} - 1\right)}}{e^{at}} \ . \tag{C 3}$$

The mixing layer Reynolds number based on the velocity difference and the vorticity thickness is thus $2U_m\delta_\omega/\nu = e^{-2at} \sqrt{1 + (e^{2at} - 1)/Re}\ (2U_0\delta_\omega^0/\nu)$. Note that in the inviscid limit $\delta_\omega/\delta_\omega^0 = e^{-at}$ and the exponential variation of the Reynolds number is split equally between the velocity difference and the vorticity thickness.

Applying the above strain at time $t = 0$ to a laminar time-developing wake with initial profile $\overline{U_1} = -U_0 e^{-4\ln 2 y^2/(b^0)^2}$, b^0 being the initial wake half width (distance between points where the wake deficit is one half its peak value) and U_0 being the initial wake deficit, results in

$$\overline{U_1} = ax - U_m \exp\left(-4\ln 2 \frac{e^{2at}}{1 + \frac{1}{Re}\left(e^{2at} - 1\right)} \frac{y^2}{(b^0)^2} \right) \tag{C 4a}$$

$$\overline{U_2} = -ay \ , \tag{C 4b}$$

where

$$U_m = U_0 \frac{e^{-at}}{\sqrt{1 + \frac{1}{Re}\left(e^{2at} - 1\right)}} \tag{C 5}$$

is the time-evolving mean wake deficit and $Re = a(b^0)^2/(8\nu\ln 2)$ is a Reynolds number. From this solution the time-evolving half width of the wake component of the flow is

$$b = b^0 \frac{\sqrt{1 + \frac{1}{Re}\left(e^{2at} - 1\right)}}{e^{at}} \ . \tag{C 6}$$

The wake Reynolds number based on the wake deficit and half width is thus $U_m b/\nu = e^{-2at}\ (U_0 b^0/\nu)$. Note that in the inviscid limit $U_m/U_0 = b/b^0 = e^{-at}$ and the exponential variation of the Reynolds number is split equally between the width and deficit, as for the self-similar solution. Both the above solutions reduce to the standard unstrained forms when a goes to zero (note that a appears in Re).

Appendix D. Turbulence modelling statistics

Reynolds-averaged statistics that may be of use for turbulence model development and additional insight into the strained wake flows are included here. Each quantity is illustrated for all ten of the flows listed in table 2.

Although Reynolds stress profiles have been presented in section 4, it is hard to obtain a clear impression of the Reynolds stress anisotropies from these plots. The time evolutions of the Reynolds stress anisotropy

$$b_{ij} = \frac{\overline{u_i' u_j'}}{q^2} - \frac{\delta_{ij}}{3} \tag{D 1}$$

and the dissipation-rate anisotropy

$$d_{ij} = \frac{\epsilon_{ij}}{2\epsilon} - \frac{\delta_{ij}}{3} \tag{D 2}$$

are plotted in figures 30 and 31, respectively. Since the anisotropies vary in the cross-stream direction, a particular cross-stream location must be chosen for the plots. Since the Reynolds shear stress $\overline{u'v'}$ is zero at the wake centreline the anisotropies are computed at the y-location (below the centreline) where $\overline{u'v'}$ reaches a maximum. For the normal Reynolds stress components, this anisotropy is similar to that at the centreline. Similarly, d_{ij} is computed at the location of maximum ϵ_{12} ($y > 0$). The cross-stream locations at which these anisotropies are being computed are thus not constant in time, nor are they constant when scaled by the wake width b (although this may be approximately the case). Irregularities in the time histories are thus usually due to changes in the location of maximum $\overline{u'v'}$, rather than sudden changes in the flow character.

Comparing figures 30 and 31, it is clear that the dissipation-rate tensor ϵ_{ij} is more isotropic than the Reynolds stress tensor $\overline{u_i' u_j'}$. In general the Reynolds stress anisotropies (associated with the large-scale turbulent motions) are not constant in time, indicating a continual change in the flow character and a lack of classical self-similarity. Possible exceptions to this include case E, in which the wake shear grows and eventually dominates the applied strain, and cases C, SC, FC, and G, in which the wake shear and applied strain remain in balance. Once these flows are developed, the anisotropy variation is less than in the other cases. The dominance of the spanwise components $\overline{w'^2}$ and ϵ_{33} at late times in cases B, F, and H is also readily apparent.

The terms in the Reynolds stress balances for each of the non-zero Reynolds stress components are shown in figures 32 to 35. Additionally, the balance for the $\overline{u_i' u_i'}$ equation is shown in figure 36. The terms plotted are as defined in equation (2.16), where both terms on the left-hand-side of the equation are plotted together (see section 3.1). The "strain" and "shear" components of the production are plotted separately, as are the turbulent and pressure diffusion components of $\mathcal{T}_{ij}$. Symbols marking the two production curves are spaced at intervals of 20 physical space grid points (on the $3N/2$ mesh used for dealiasing). The viscous diffusion terms $\mathcal{V}_{ij}$ are not plotted because they are all an order of magnitude smaller than the other terms in the balance and would not be visible on the scale used in the figures. The balances are shown at a time $a(t - t_1) \approx 1.2$, when the flows are developed but not overly constrained by computational box size limitations.

As discussed in section 3.3 and noted for the Reynolds stress profiles presented in figure 11, profiles for flows in which the computational domain size becomes limited are noisy. The smoothest profiles are observed in cases A, D and G, in which the size of the x-z domain increases in time and a larger and larger domain is available for generating average statistics. Cases B, C, SC, and H, in which the x-z domain is reduced in time,

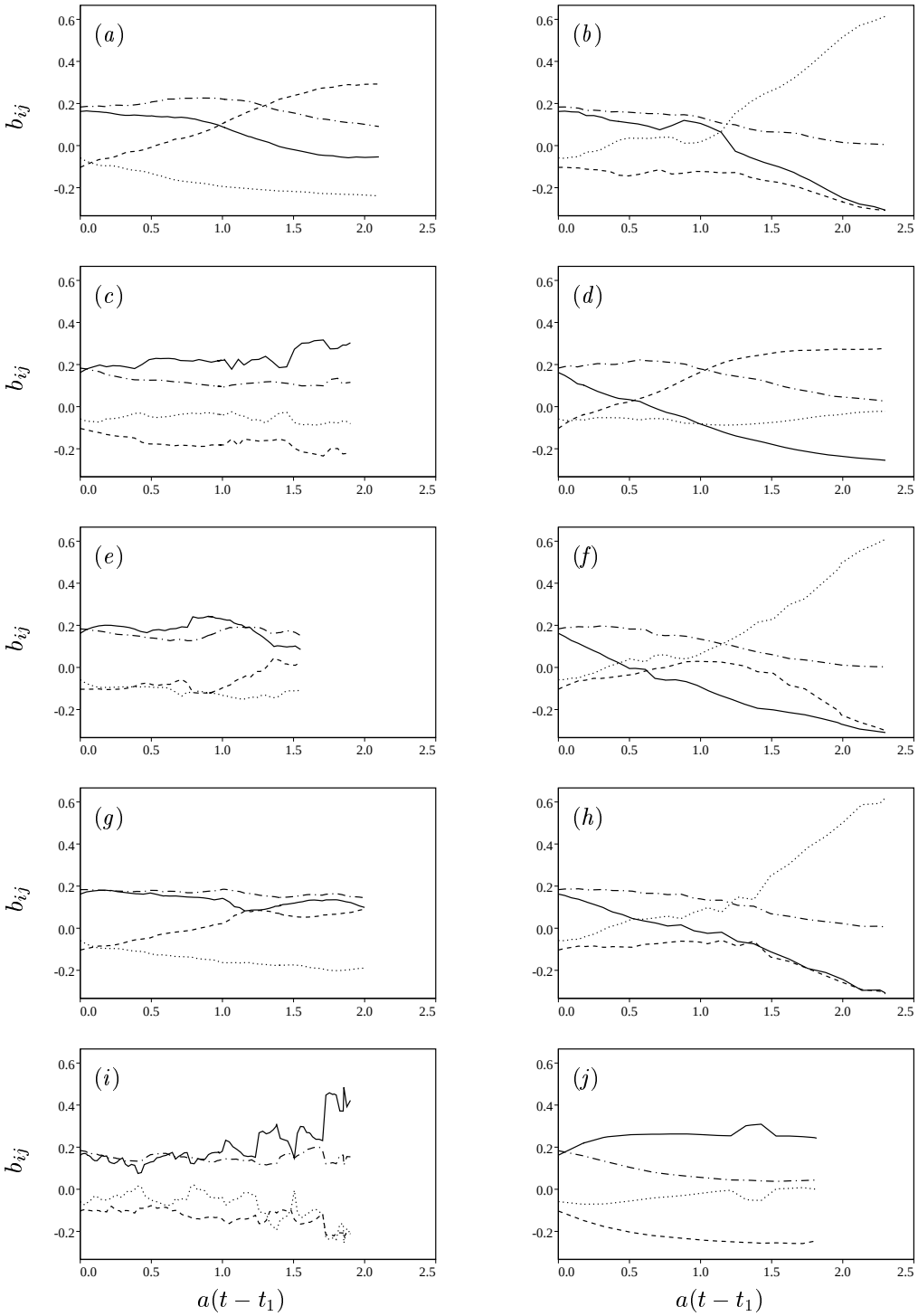

FIGURE 30. Time evolution of Reynolds stress anisotropy b_{ij} at the y-location with maximum $\overline{u'v'}$ for (a) case A, (b) case B, (c) case C, (d) case D, (e) case E, (f) case F, (g) case G, (h) case H, (i) case SC, and (j) case FC. —— b_{11}, – – – b_{22}, ····· b_{33}, and —·— b_{12}.

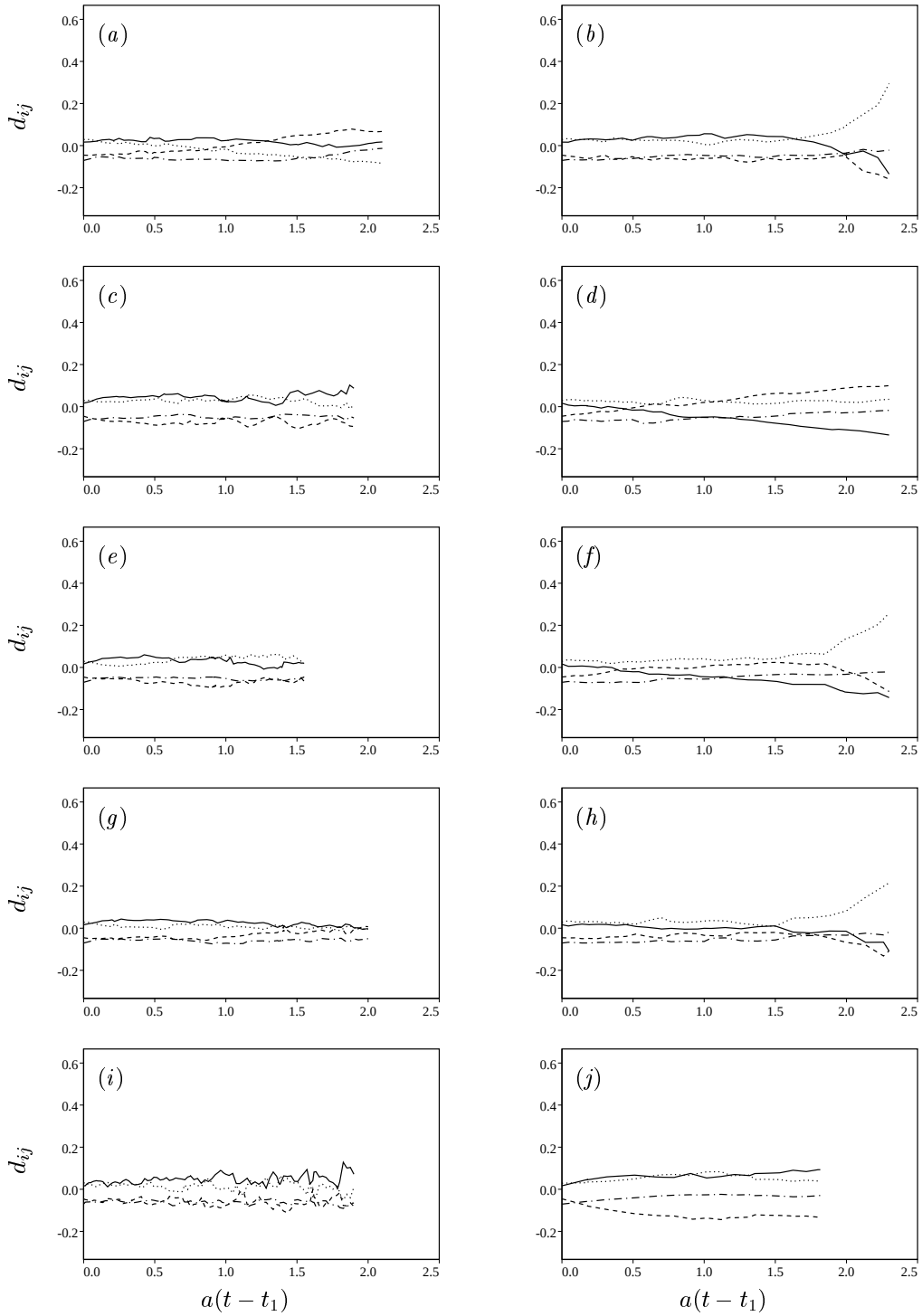

FIGURE 31. Time evolution of the dissipation-rate anisotropy d_{ij} at the y-location with maximum ϵ_{12} for (a) case A, (b) case B, (c) case C, (d) case D, (e) case E, (f) case F, (g) case G, (h) case H, (i) case SC, and (j) case FC. ——— d_{11}, – – – – d_{22}, ····· d_{33}, and —·— d_{12}.

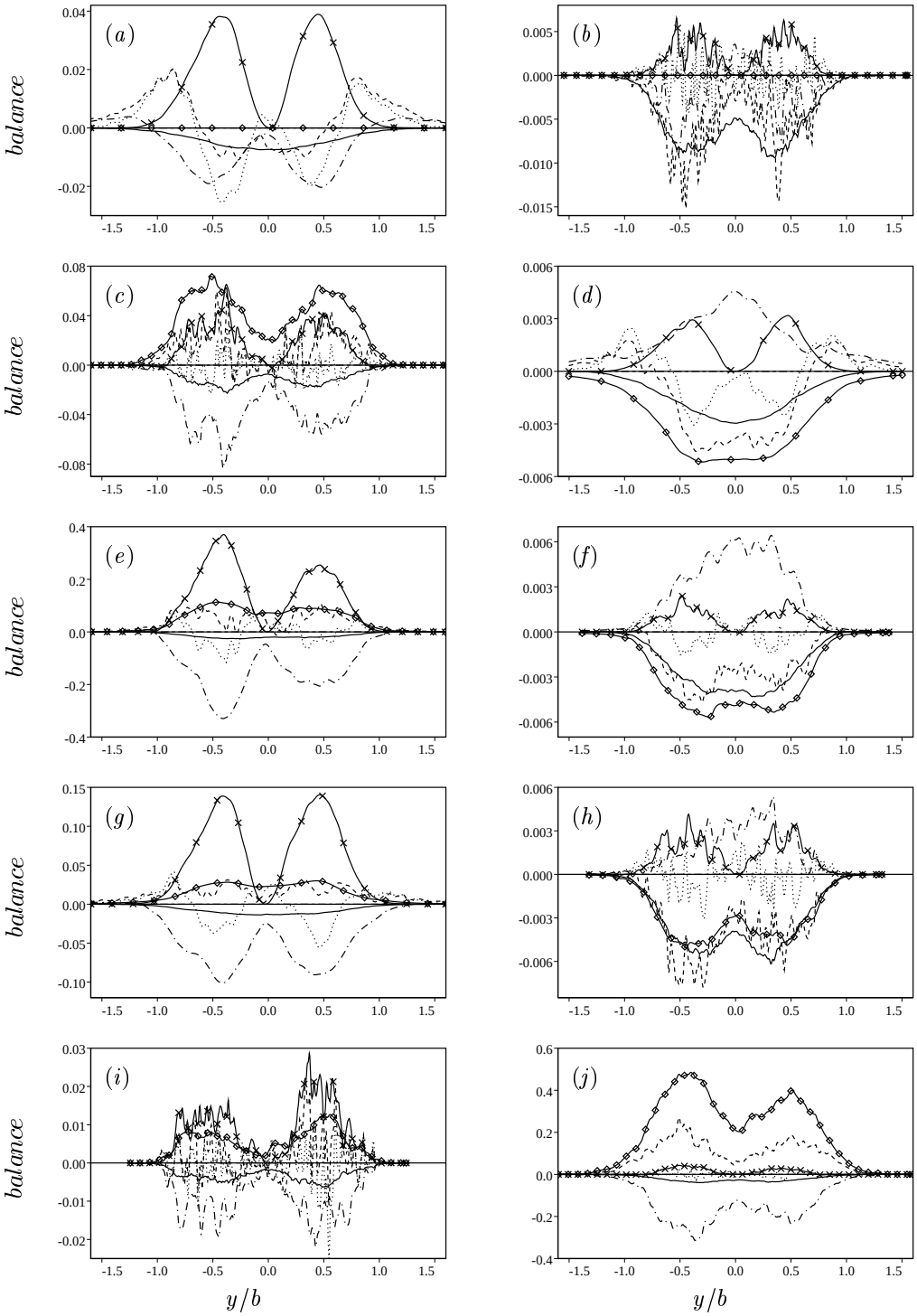

FIGURE 32. Profiles of terms in the Reynolds stress budget (2.16) for the $\overline{u'^2}$ equation for (a) case A, (b) case B, (c) case C, (d) case D, (e) case E, (f) case F, (g) case G, (h) case H, (i) case SC, and (j) case FC at $a(t-t_1) \approx 1.2$. ---- $\partial\overline{u'^2}/\partial t + a_{22}y\ \partial\overline{u'^2}/\partial y$, ——— $\times$ shear production part of $\mathcal{P}_{11}$, ——— $\diamond$ strain production part of $\mathcal{P}_{11}$, ····· turbulent diffusion (first part of $\mathcal{T}_{11}$), —·— pressure strain $\mathcal{W}_{11}$, and ——— dissipation ϵ_{11}. The pressure diffusion terms are zero in the $\overline{u'^2}$ equation. The viscous diffusion terms $\mathcal{V}_{11}$ are an order of magnitude smaller than the other terms in the balance and cannot be seen at this scale.

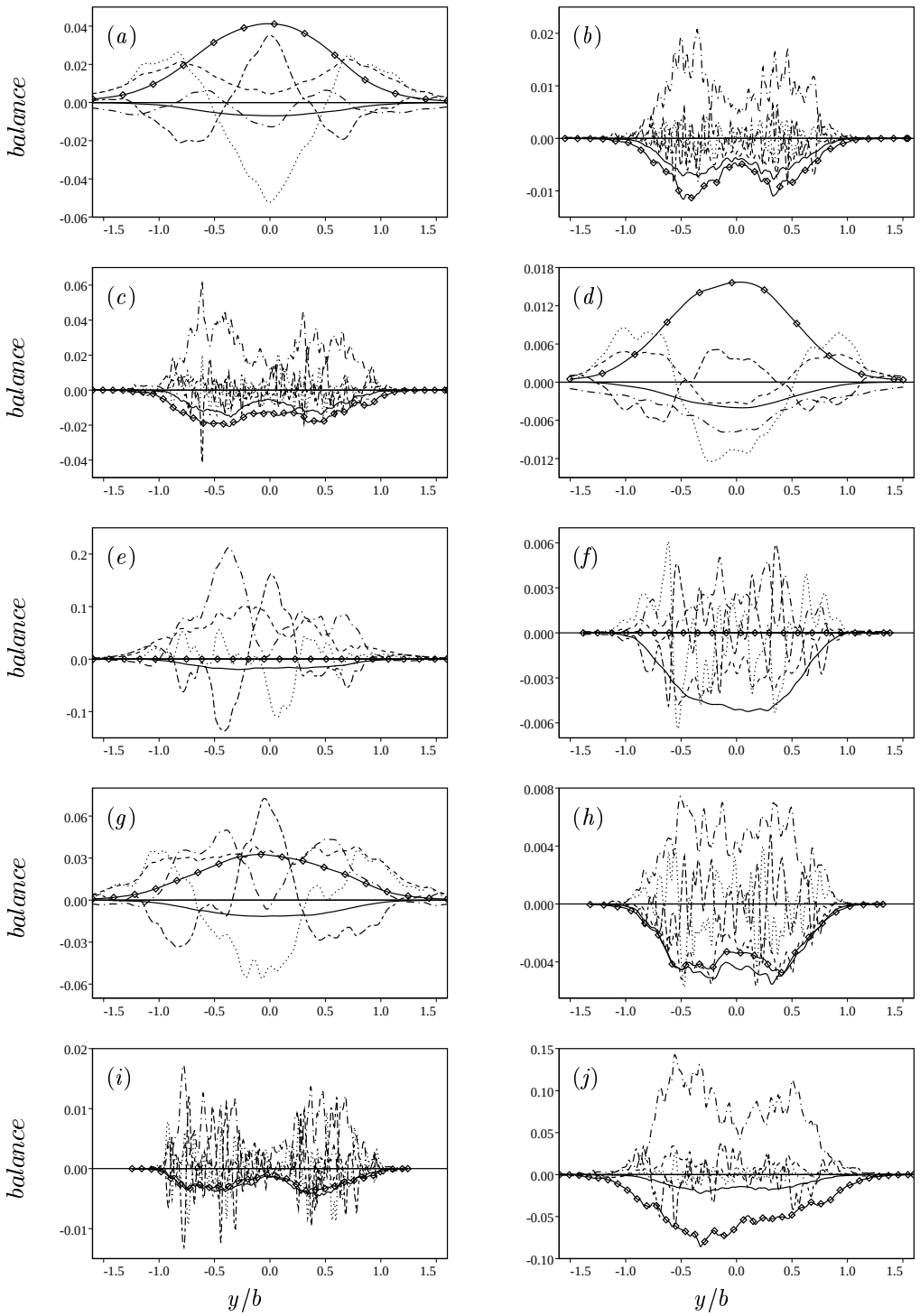

FIGURE 33. Profiles of terms in the Reynolds stress budget (2.16) for the $\overline{v'^2}$ equation for (a) case A, (b) case B, (c) case C, (d) case D, (e) case E, (f) case F, (g) case G, (h) case H, (i) case SC, and (j) case FC at $a(t-t_1) \approx 1.2$. ---- $\partial\overline{v'^2}/\partial t + a_{22}y\ \partial\overline{v'^2}/\partial y$, ——— $\diamond$ strain production part of $\mathcal{P}_{22}$, ····· turbulent diffusion (first part of $\mathcal{T}_{22}$), —·— pressure diffusion (pressure terms in $\mathcal{T}_{22}$), —·—·— pressure strain $\mathcal{W}_{22}$, and ——— dissipation ϵ_{22}. The viscous diffusion terms $\mathcal{V}_{22}$ are an order of magnitude smaller than the other terms in the balance and cannot be seen at this scale.

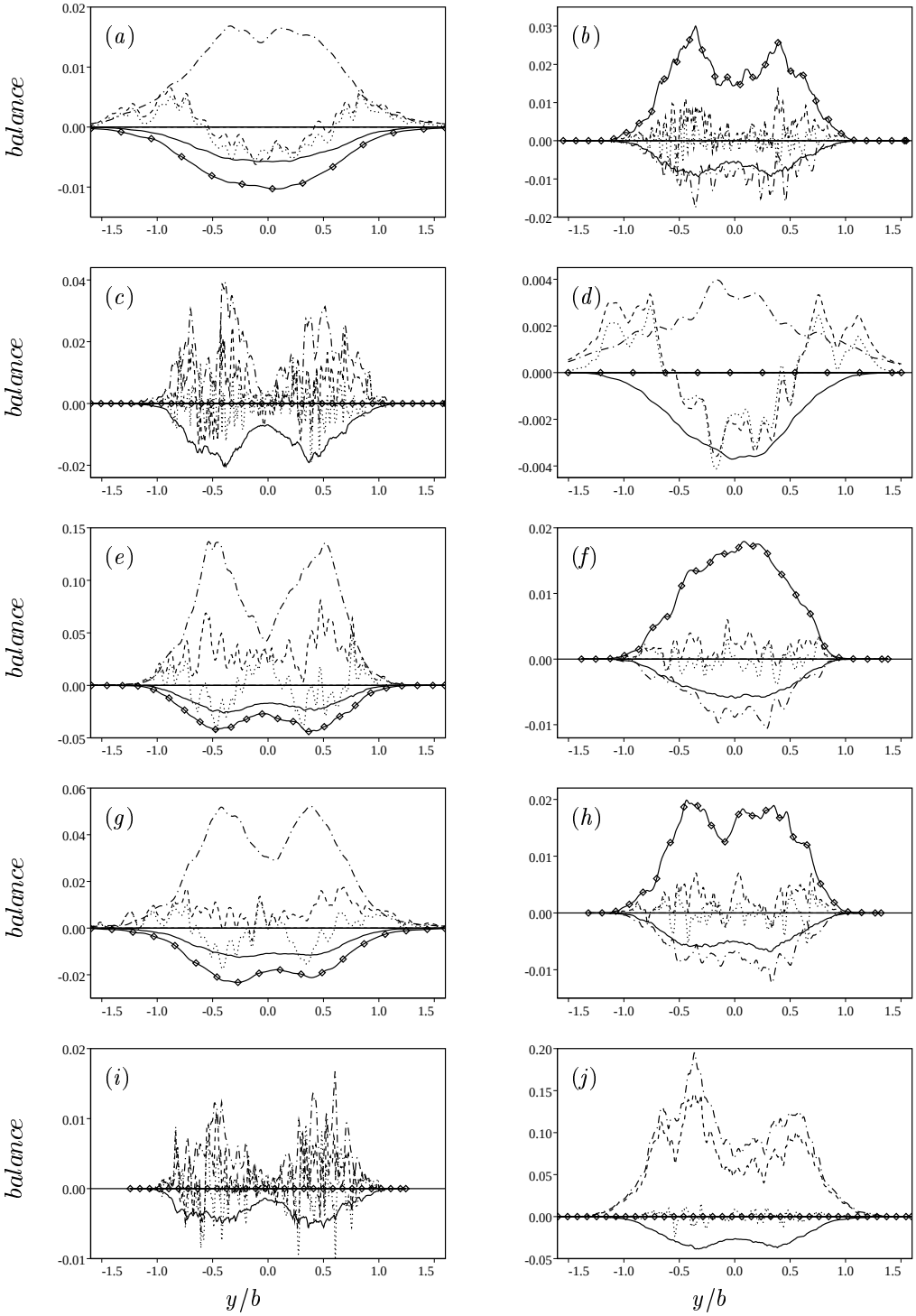

FIGURE 34. Profiles of terms in the Reynolds stress budget (2.16) for the $\overline{w'^2}$ equation for (a) case A, (b) case B, (c) case C, (d) case D, (e) case E, (f) case F, (g) case G, (h) case H, (i) case SC, and (j) case FC at $a(t-t_1) \approx 1.2$. - - - - $\partial\overline{w'^2}/\partial t + a_{22}y\ \partial\overline{w'^2}/\partial y$, ——— $\diamond$ strain production part of $\mathcal{P}_{33}$, ····· turbulent diffusion (first part of $\mathcal{T}_{33}$), —·— pressure strain $\mathcal{W}_{33}$, and ——— dissipation ϵ_{33}. The pressure diffusion terms are zero in the $\overline{w'^2}$ equation. The viscous diffusion terms $\mathcal{V}_{33}$ are an order of magnitude smaller than the other terms in the balance and cannot be seen at this scale.

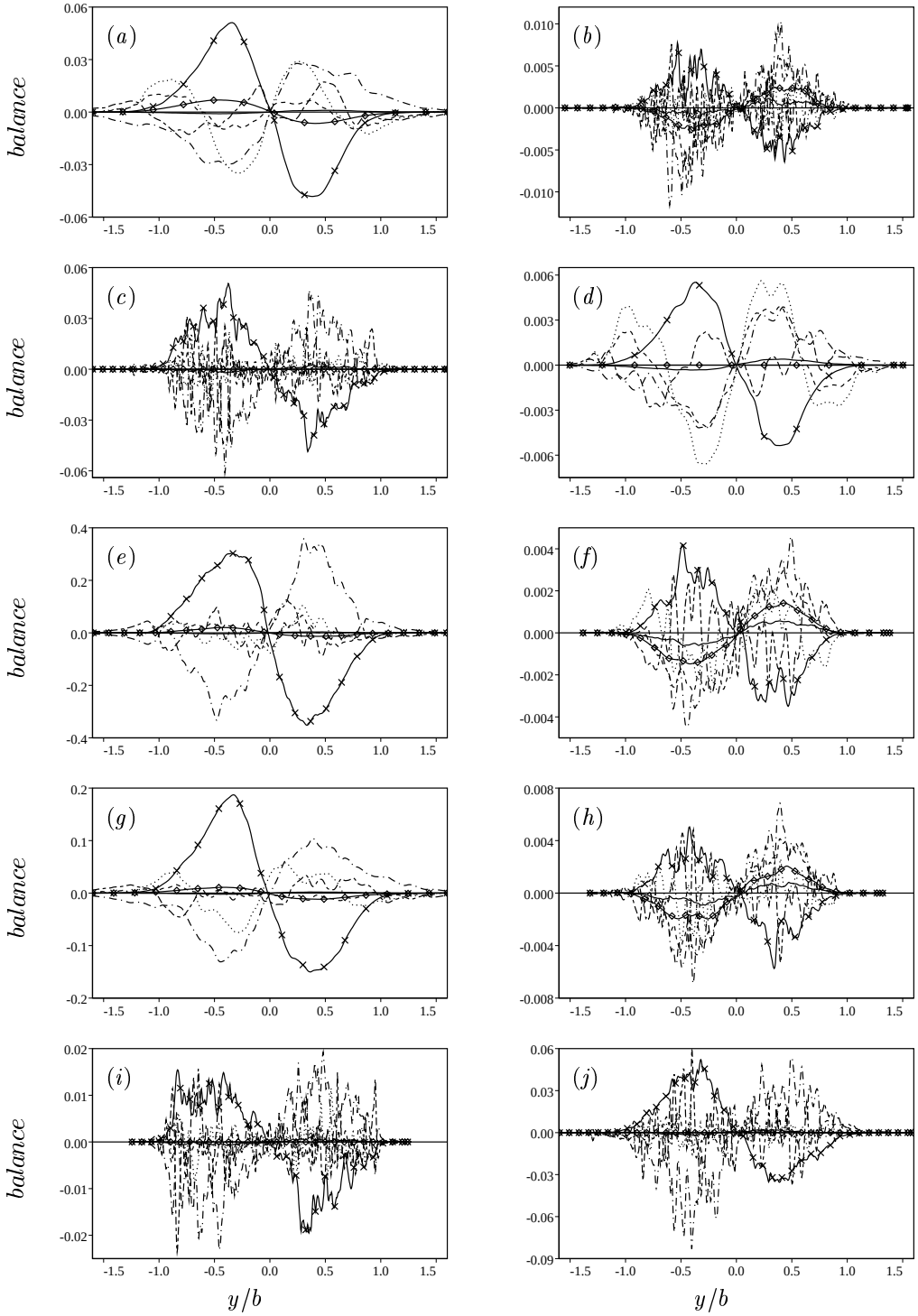

FIGURE 35. Profiles of terms in the Reynolds stress budget (2.16) for the $\overline{u'v'}$ equation for (a) case A, (b) case B, (c) case C, (d) case D, (e) case E, (f) case F, (g) case G, (h) case H, (i) case SC, and (j) case FC at $a(t-t_1) \approx 1.2$. – – – – $\partial\overline{u'v'}/\partial t + a_{22}y\,\partial\overline{u'v'}/\partial y$, ——— $\times$ shear production part of $\mathcal{P}_{12}$, ——— $\diamond$ strain production part of $\mathcal{P}_{12}$, ····· turbulent diffusion (first part of $\mathcal{T}_{12}$), — – — pressure diffusion (pressure terms in $\mathcal{T}_{12}$), —·— pressure strain $\mathcal{W}_{12}$, and ——— dissipation ϵ_{12}. The viscous diffusion terms $\mathcal{V}_{12}$ are an order of magnitude smaller than the other terms in the balance and cannot be seen at this scale.

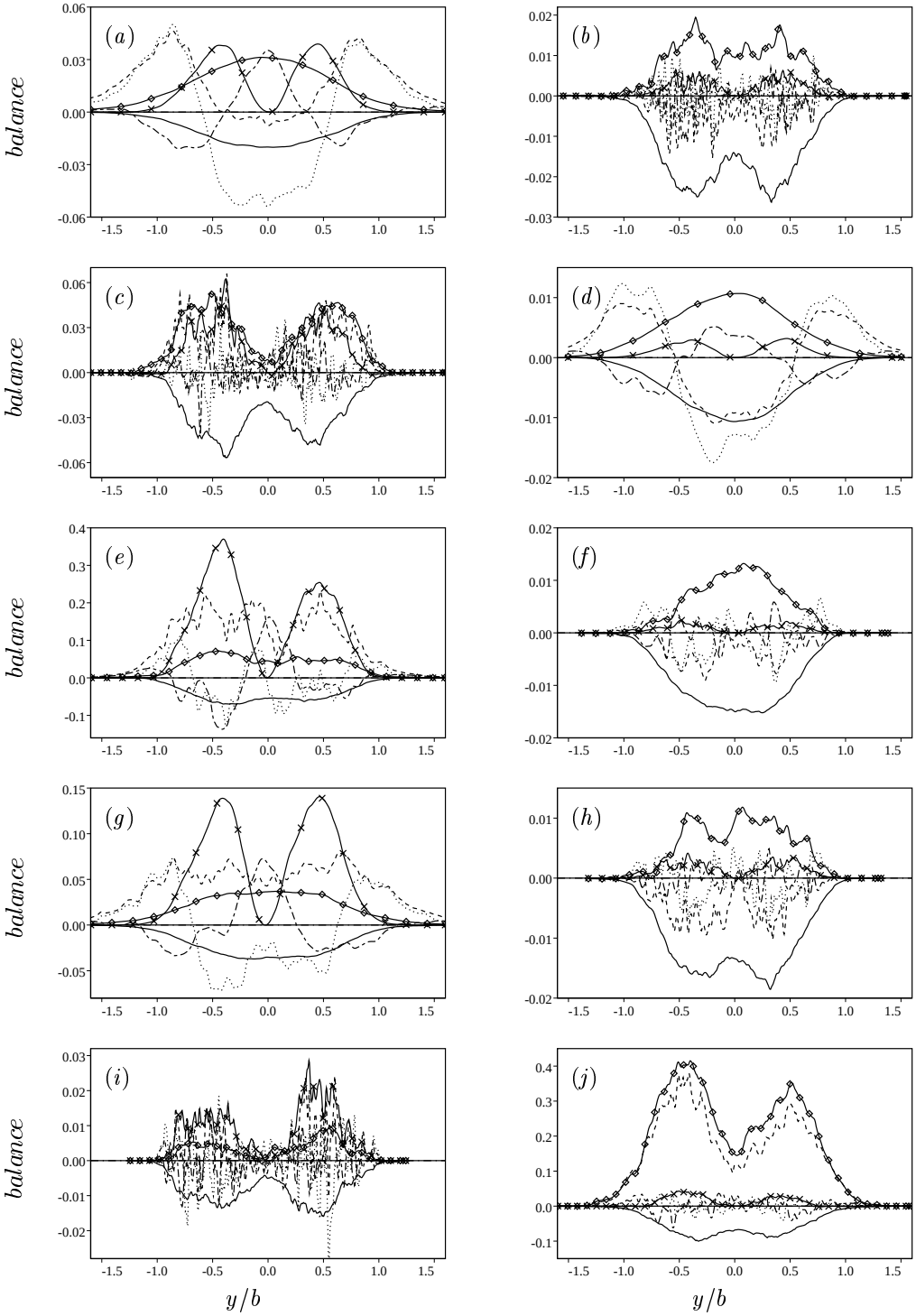

FIGURE 36. Profiles of terms in the Reynolds stress budget (2.16) for the $\overline{u_i'u_i'}$ equation for (*a*) case A, (*b*) case B, (*c*) case C, (*d*) case D, (*e*) case E, (*f*) case F, (*g*) case G, (*h*) case H, (*i*) case SC, and (*j*) case FC at $a(t-t_1) \approx 1.2$. ---- $\partial\overline{u_i'u_i'}/\partial t + a_{22}y\ \partial\overline{u_i'u_i'}/\partial y$, ——— $\times$ shear production part of $\mathcal{P}_{ii}$, ——— $\diamond$ strain production part of $\mathcal{P}_{ii}$, ····· turbulent diffusion (first part of $\mathcal{T}_{ii}$), — — — pressure diffusion (pressure terms in $\mathcal{T}_{ii}$), and ——— dissipation ϵ_{ii}. The viscous diffusion terms $\mathcal{V}_{ii}$ are an order of magnitude smaller than the other terms in the balance and cannot be seen at this scale.

show the noisiest statistics. Despite the shrinking x-z domain in case FC, the profiles are reasonably smooth, perhaps because of the shorter evolution time for this rapidly strained case.

Since the flow evolution is not yet completely self-similar through to the level of the Reynolds stresses, these balances will be different at other times. Also, it is unclear how to scale the data in the absence of self-similarity. Here the abscissa has been scaled as y/b. As can be seen from the results presented in section 4 and the experiments of Reynolds (1962) and Keffer (1965), the width of the various Reynolds stress profiles remains proportional to the width of the wake and the scaling y/b should thus do a reasonable job of collapsing the data from the various cases. This is indeed the case, as can be seen from the balance figures, which all cover the same range $-1.6 < y/b < 1.6$. The cases with cross-stream compression (A, D, and to a lesser extent G) show significant Reynolds stress levels out to slightly larger values of y/b, but in general the profile widths from the various cases are similar. On the other hand, the classical self-similar scaling for the balance terms, U_m^3/b, increases the spread among the cases (compare figure 15b with figure 15a) and is not helpful for these flows. For this reason the balance terms are scaled by the initial value $(U_m^0)^3/b^0$, rather than by U_m^3/b.

Reynolds (1962) argued that self-similarity would only be achieved for strained wakes in which the turbulence production by the wake shear was larger than that by the applied strain. While the later experiments by Keffer (1965) and the results presented here indicate that the classical self-similarity Reynolds sought does not occur, it is still of interest to examine the relative importance of these two production terms. Production of turbulent kinetic energy by the wake shear occurs entirely in the $\overline{u'^2}$ component. For cases A and B this component is not produced by the strain ($a_{11} = 0$) and the shear production obviously dominates. The shear production also dominates in case E, where the shear rate is increasing as a result of the straining, and in cases G and SC, where the applied a_{11} strain rate is reduced. In cases D, F, and H the wake shear rate decreases in time and the magnitude of the strain "production" of $\overline{u'^2}$ (actually a destruction term since $a_{11} > 0$) is greater than that of the (positive) shear production (note that more than enough strain production occurs in the other normal Reynolds stress components to offset this negative strain production, see the following discussion of the q^2 balance). In case C the shear rate and strain rate remain in balance, but the strain production of $\overline{u'^2}$ is larger than the shear production (although the turbulent kinetic energy is reduced to some extent by negative strain production of $\overline{v'^2}$). The dominance of strain production is more apparent in case FC, in which the strain rate is four times larger. It should be noted that even when the strain rate is reduced by a factor of four (case SC) the strain production remains significant, although smaller than the shear production.

As with the $\overline{u'^2}$ balances, the shear production of q^2 dominates the strain production when the strain rate is low (cases SC and G) or the wake shear rate increases in time (case E). In case A (delayed decay of the wake shear) and case C (no decay of the wake shear) the two production terms are similar in magnitude. In the remaining 5 cases the strain production dominates, either as a result of decaying wake shear or high strain rate. As can be seen in figure 36, the total contribution from the strain "production" of q^2 (which includes negative production in at least one normal Reynolds stress component) is always positive. Despite this, changes in other terms in the balances result in decreased levels of q^2 compared to those in the unstrained wake in case D and for early times in cases B, F and H. (see figure 14a).

For all the flows simulated, production of the Reynolds shear stress $\overline{u'v'}$ is always dominated by the wake shear production, even for the flows in which the wake shear is

decaying. For cases B, F, and H (spanwise compression) the strain "production" actually reduces Reynolds shear stress. Note that the dissipation of Reynolds shear stress ϵ_{12} is small, with most of the dissipation actually being accomplished by the pressure-strain term.

A number of other interesting observations about the other terms in the Reynolds stress balance can be made from examination of these figures. For instance, it appears that the turbulent diffusion is negligible for cases B and C (and SC and FC), perhaps as a result of the lack of large-scale organization in these flows that are rapidly stretched in the cross-stream direction. The noisy profiles makes it difficult to draw firm conclusions for these cases, however.